Article

Cell

Mutational Strand Asymmetries in Cancer Genomes Reveal Mechanisms of DNA Damage and Repair

Graphical Abstract

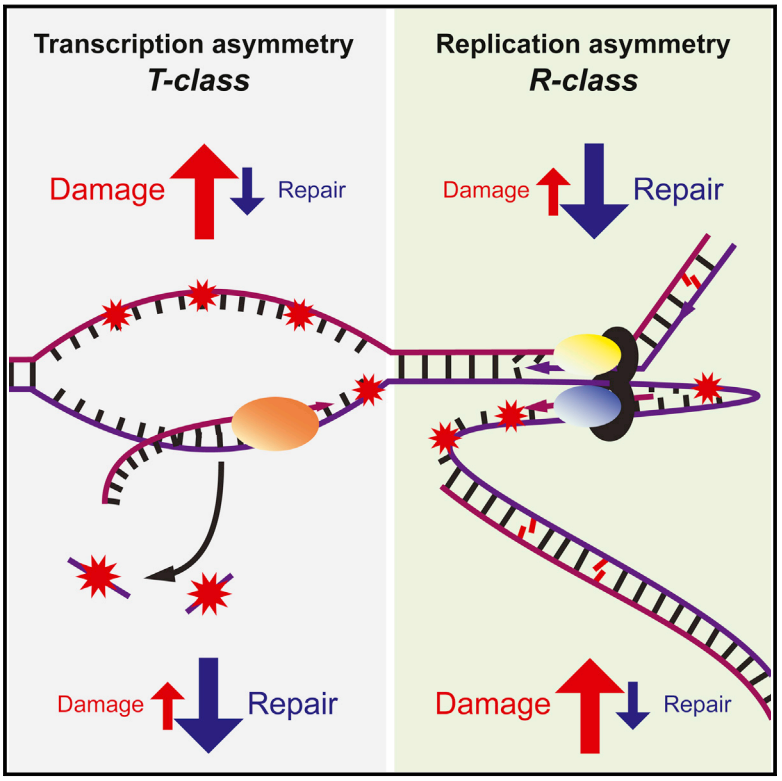

Highlights

- Replicative and transcriptional mutational asymmetries are widespread across cancer
- APOBEC mutagenesis in humans primarily occurs on the lagging-strand template
- Mismatch repair balances asymmetric replication errors
- Transcription-coupled damage (TCD) introduces sense-strand mutations in liver cancer

Authors

Nicholas J. Haradhvala, Paz Polak, Petar Stojanov, ..., Amnon Koren, Michael S. Lawrence, Gad Getz

Correspondence

lawrence@broadinstitute.org (M.S.L.), gadgetz@broadinstitute.org (G.G.)

In Brief

Using an approach that distinguishes whether mutations in cancer genomes occurred on the transcribed or non-transcribed DNA strand with respect to transcription and on the leading or lagging strand with respect to replication, the predominant mutational mechanisms associated with different types of cancers and mutational patterns can be inferred.

Haradhvala et al., 2016, Cell *164*, 538–549
January 28, 2016 ©2016 Elsevier Inc.
http://dx.doi.org/10.1016/j.cell.2015.12.050

CellPress

Cell

Article

Mutational Strand Asymmetries in Cancer Genomes Reveal Mechanisms of DNA Damage and Repair

Nicholas J. Haradhvala,[1,2,8] Paz Polak,[1,2,3,8] Petar Stojanov,[4] Kyle R. Covington,[5] Eve Shinbrot,[5] Julian M. Hess,[2] Esther Rheinbay,[1,2] Jaegil Kim,[2] Yosef E. Maruvka,[1,2] Lior Z. Braunstein,[2] Atanas Kamburov,[1,2,3] Philip C. Hanawalt,[6] David A. Wheeler,[5] Amnon Koren,[2,7] Michael S. Lawrence,[2,9,*] and Gad Getz[1,2,3,9,*]

[1]Massachusetts General Hospital Cancer Center and Department of Pathology, 55 Fruit Street, Boston, MA 02114, USA
[2]Broad Institute of Harvard and MIT, 415 Main Street, Cambridge, MA 02142, USA
[3]Harvard Medical School, 25 Shattuck Street, Boston, MA 02115, USA
[4]Carnegie Mellon University School of Computer Science, 5000 Forbes Avenue, Pittsburgh, PA 15213, USA
[5]Baylor College of Medicine, 1 Baylor Plaza, Houston, TX 77030, USA
[6]Stanford University Department of Biology, 450 Serra Mall, Stanford, CA 94305, USA
[7]Cornell University Department of Molecular Biology and Genetics, 526 Campus Road, Ithaca, NY 14853, USA
[8]Co-first author
[9]Co-senior author
*Correspondence: lawrence@broadinstitute.org (M.S.L.), gadgetz@broadinstitute.org (G.G.)
http://dx.doi.org/10.1016/j.cell.2015.12.050

SUMMARY

Mutational processes constantly shape the somatic genome, leading to immunity, aging, cancer, and other diseases. When cancer is the outcome, we are afforded a glimpse into these processes by the clonal expansion of the malignant cell. Here, we characterize a less explored layer of the mutational landscape of cancer: mutational asymmetries between the two DNA strands. Analyzing whole-genome sequences of 590 tumors from 14 different cancer types, we reveal widespread asymmetries across mutagenic processes, with transcriptional ("T-class") asymmetry dominating UV-, smoking-, and liver-cancer-associated mutations and replicative ("R-class") asymmetry dominating POLE-, APOBEC-, and MSI-associated mutations. We report a striking phenomenon of transcription-coupled damage (TCD) on the non-transcribed DNA strand and provide evidence that APOBEC mutagenesis occurs on the lagging-strand template during DNA replication. As more genomes are sequenced, studying and classifying their asymmetries will illuminate the underlying biological mechanisms of DNA damage and repair.

INTRODUCTION

A thorough understanding of mutational density and patterns in cancer genomes is important for studying the mechanisms of mutagenesis (Pleasance et al., 2010a, 2010b), for modeling the evolution of cancer genomes (Alexandrov et al., 2013; Nik-Zainal et al., 2012b), and for identifying cancer genes (Lawrence et al., 2013). In cancer genomes, somatic mutations exhibit heterogeneity in total mutation density, in mutation spectra among tumors and cancer types, and in mutation density along the genome within a given tumor (Lawrence et al., 2013; Pleasance et al., 2010a, 2010b). This heterogeneity is caused by underlying mutational processes that reflect different genetic backgrounds and mutagenic exposures and by a non-uniform epigenomic landscape with variation in DNA replication timing, chromatin structure, and gene expression levels across the genome (Lawrence et al., 2013; Pleasance et al., 2010a, 2010b; Polak et al., 2014, 2015; Waddell et al., 2015).

One challenge inherent in the analysis of genomic mutations is the loss of strand information that occurs between the initial occurrence of a mutagenic lesion and the ultimate readout by DNA sequencing. For instance, consider a mutational process whose initiating event is oxidative attack on the guanine of a C:G base pair. In principle, if we isolated the DNA immediately after such an attack, we could directly observe the lesion; however, in genomic sequencing data, we don't encounter mutations until many cell divisions later. The result of such a lesion is generally an A:G mismatch after the first cell division, leading to a stable A:T base pair after an additional round of replication. Since approximately half of C:G base pairs are oriented with the cytosine on the reference (Watson) and half on the anti-reference (Crick) strand, roughly equal numbers of "G→T" and "C→A" mutations are seen. A lesion at the cytosine of a C:G base pair could produce exactly the same result, so working backward, we cannot determine the base of the original DNA damage. This is because using the genomic reference strand as the "frame of reference" for base-pair orientation is merely an arbitrary convention.

However, we can recover some strand information by considering a more biologically meaningful reference frame. In regions that undergo DNA transcription, the DNA can be oriented with respect to the transcribed strand. Thus, we would consider a C:G→A:T base pair change to be a "C→A" or "G→T" mutation

depending on whether the C or the G is in the template strand for transcription. Alternatively, we can use DNA replication to define a frame of reference. In this case, whether the C of a C:G base pair is on the leading or the lagging strand of DNA replication would determine the type of mutation. Because replication and transcription are each associated with opportunities for the asymmetric (strand-specific) introduction and repair of DNA damage, they each have the potential to leave their footprints in a patient's mutational profile in the form of unequal rates and patterns of mutations on the two strands of DNA (Francioli et al., 2015; Green et al., 2003; Lobry, 1996; Lujan et al., 2012; Pleasance et al., 2010a, 2010b; Polak and Arndt, 2008; Polak et al., 2010; Shinbrot et al., 2014; Touchon et al., 2005).

Strand asymmetry has already been well studied in the context of transcription. DNA lesions encountered on the transcribed ("template") strand can stall progression of the RNA polymerase, leading to the recruitment of a nucleotide excision repair (NER) complex that can correct the damage (Donahue et al., 1994; Fousteri and Mullenders, 2008; Hanawalt and Spivak, 2008; Jiang and Sancar, 2006; Mellon et al., 1987; Spivak and Ganesan, 2014). Importantly, higher transcription levels of a gene are associated with more opportunities for transcription-coupled repair (TCR), leading to an inverse correlation between the expression level of a gene and its mutation density (Chapman et al., 2011; Lawrence et al., 2013; Pleasance et al., 2010a). Conversely, damage on the non-template ("sense") strand may fail to stall the RNA polymerase and therefore could escape repair by TCR. In addition, the non-template strand remains single-stranded during the process of transcription and is therefore more vulnerable to damage (Jinks-Robertson and Bhagwat, 2014). In combination, these mechanisms lead to differences in mutation densities and spectra on the transcribed and non-transcribed strands (Pleasance et al., 2010a, 2010b). Notably, transcriptional strand asymmetry provides information regarding damage and TCR beyond what can be gathered from the correlation of mutational densities with expression, since the latter is convolved with other genomic factors such as chromatin-state- and replication-timing-dependent mismatch repair (MMR; Supek and Lehner, 2015).

Strand asymmetry can also be viewed in the reference frame of DNA replication. The DNA replication fork is composed of a leading strand, copied in a largely continuous fashion, and a lagging strand, copied as a discontinuous series of Okazaki fragments. DNA polymerases α, δ, and ε work together to replicate the DNA but have distinct roles in synthesis and proofreading. The resulting asymmetry reflects an imbalance in the types of mutations introduced on the leading versus lagging strand, although it is still a matter of debate whether this occurs due to the division of labor of distinct polymerases in DNA synthesis (Miyabe et al., 2011; Nick McElhinny et al., 2008) or due to specialized polymerase proofreading properties (Johnson et al., 2015; Stillman, 2015). Additionally the lagging strand endures longer exposure as single-stranded DNA (ssDNA; Yu et al., 2014) and, as such, may be more vulnerable to ssDNA-targeting mutagens. These factors lead to replication-associated mutational asymmetry that flips (i.e., inverts which strand has the higher mutation density) at replication origins. Replication-strand asymmetries were observed as local skews in nucleotide composition in the chromosomes of bacterial (Lobry, 1996; McLean et al., 1998) and eukaryotic (Touchon et al., 2005) species, are associated with robustly programmed yeast replication origins (Koren et al., 2010), and have also been experimentally demonstrated in yeast (Lujan et al., 2012; Pavlov et al., 2002).

RESULTS

A Framework for Analysis of Replicative and Transcriptional Asymmetries

We partitioned the human genome in two ways: first, by transcription direction, using RefSeq gene definitions (Figure 1A). We annotated genomic regions as tx(+) when they encoded genes on the reference strand and as tx(−) when they encoded genes on the complementary strand. We considered the patterns of mutations in smoking-associated lung cancers, combining mutation data from seven lung adenocarcinomas (LUAD) that exhibited a strong smoking signature. Mutational densities of C:G→A:T are highest in both tx(+) and tx(−) genes when the guanine is on the non-transcribed strand (Figure 1C). This is consistent with the known mechanism of the smoking signature, driven by carcinogen attack at guanines (Denissenko et al., 1996). TCR lowers the mutational densities of C:G base pairs in which the guanine serves as the transcription template (denoted C_{ntx}:G_{tx}), relative to intergenic regions (IGR). In contrast, G_{ntx}:C_{tx} base pairs do not benefit from this extra opportunity for repair, resulting in undiminished mutation density of G_{ntx}:C_{tx}→T_{ntx}:A_{tx}, as shown previously (Pleasance et al., 2010b).

The second form of genome partitioning was by DNA replication direction. Since the entire genome is replicated every time a cell divides (but only a portion is transcribed), replication direction has the potential to exert larger asymmetries in mutational data. However, determining direction is much more challenging for replication than transcription, since the precise locations of replication origins in the human genome are not known. This has precluded a comprehensive analysis of replicative strand asymmetry thus far.

To enable an analysis of replication direction and strand asymmetry, we utilized high-resolution genomic replication timing data from deep DNA sequencing of S- and G1-phase cells from lymphoblastoid cell lines of six individuals (Koren et al., 2012). These data exhibit valleys and peaks in a timing-versus-location landscape that correspond to the approximate locations of replication origins (or origin clusters) and replication termini (Figure 1B). The regions between valleys and peaks correspond, in principle, to regions that replicate predominantly in a single direction (from origin to termination zone) and for which predominant replication direction can be assigned. This approach has previously been used to reveal compositional skews and asymmetric evolutionary germline mutations in the human genome (Chen et al., 2011). However, there are inherent limitations in the identification of replication origins based on replication timing valleys, and there is a lack of a gold standard (i.e., a set of replication origins with known locations) with which to benchmark this approach.

The valleys and peaks (constant-timing regions) are the source of most tissue-specific variation in the profiles (Rhind and

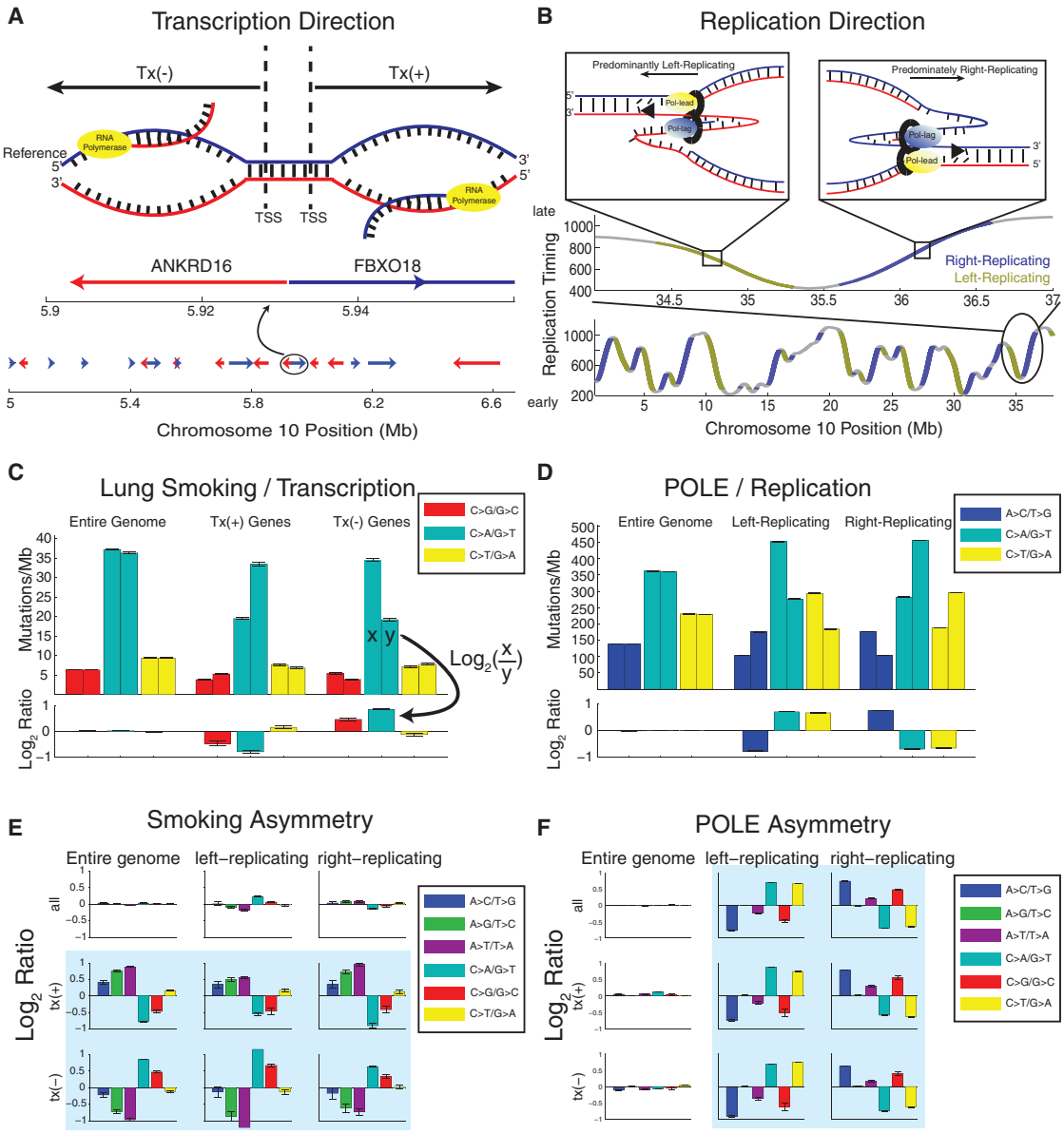

Figure 1. Mutational Strand Asymmetry Associated with Transcription and Replication

Transcription is shown on the left and replication on the right.

(A) Transcription direction: Tx(+) regions carry the coding sequence of a gene on the genomic reference strand, and Tx(−) regions carry the coding sequence on the genomic complement strand.

(B) Replication direction: positive slope in replication timing data indicates general rightward movement of the replication complex ("right-replicating"), while negative slope indicates left-replicating.

(C) Lung cancers show strong transcriptional ("T-class") asymmetry. Each pair of bars (upper axis) shows the density of mutations at C:G (left bar) and G:C (right bar) base pairs. When summing across the entire genome, base-pair orientation does not affect mutational densities. In tx(+) regions, G:C base pairs show a higher density of G→T transversions than C:G base pairs; the opposite is true in tx(−) regions. Lower axis shows the $\log_2$ ratio of each pair of bars.

(D) POLE mutant cancers (colorectal and endometrial) show strong replicative ("R-class") asymmetry. Left-replicating regions show a higher density of mutations at C:G base pairs, and right-replicating regions show a higher density at G:C.

(E) Lung cancers show strong T-class asymmetry but little R-class.

(F) POLE mutant cancers show strong R-class strand asymmetry but little T-class.

Error bars represent 95% confidence interval.

Gilbert, 2013; Ryba et al., 2010) and, furthermore, present no clear direction of replication. Therefore, we excluded these regions from our analysis and focused on "timing transition regions" (TTRs), which are highly conserved (Rhind and Gilbert, 2013; Ryba et al., 2010) and have a prominent slope that indicates the general direction of replication, either "left-replicating"

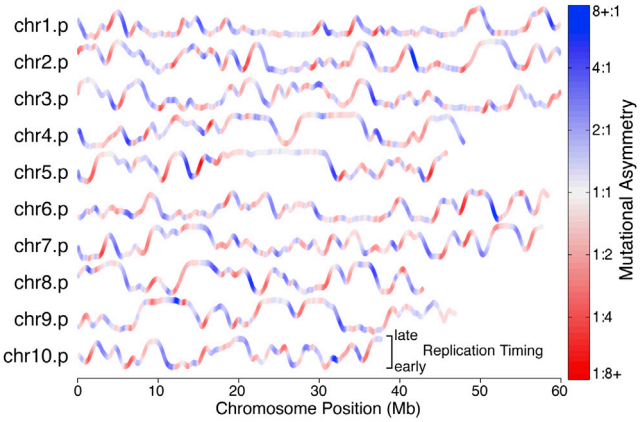

Figure 2. Strand Asymmetry in POLE Mutant Cancers Reflects Directionality of DNA Replication TTRs

Replication timing profiles are shown for the p arms (up to 60 Mb) of the first ten chromosomes. Profiles are colored by the local ratio of C→A to G→T mutations in a cohort of 12 mutant-POLE genomes (colorectal and endometrial). Strikingly, late-to-early TTRs (where slope is negative) frequently have a strong bias toward C→A mutations (blue), consistent with leading-strand synthesis using the reference strand as template. Conversely, early-to-late TTRs (positive slopes) show bias toward G→T mutations (red), consistent with lagging-strand synthesis using the reference strand as template (Shinbrot et al., 2014).

or "right-replicating." (We use the terms "left" and "right" when viewing the DNA in the standard orientation.) While TTRs were first thought to represent regions that are entirely uni-directional in replication (Ryba et al., 2010), it was later suggested that the vast majority of these regions are replicated too quickly for a single replication fork and are more likely replicated by origins that fire in close succession (Guilbaud et al., 2011; Rhind and Gilbert, 2013). For any pair of sequentially firing origins, the greater portion of the inter-origin distance is replicated by the fork originating from the earlier of the two origins. The result is that, in aggregate, the larger portion of a TTR is synthesized in the early-to-late direction (Figure S1). Thus, TTRs have a predominant replication direction given by the sign of their slope. Restricting analysis to these regions enabled us to assign the predominant replication direction to 38% of the genome.

To validate our ability to measure replicative asymmetry using these left- and right-replicating definitions, we considered the one known case of replicative mutational asymmetry: tumors carrying functional mutations in the proofreading exonuclease domain of *POLE*, the gene encoding polymerase ε (designated as "POLE tumors"; Shinbrot et al., 2014). The exonuclease domain of polymerase ε is responsible for proofreading during synthesis of the leading strand (Nick McElhinny et al., 2008; Shinbrot et al., 2014), and POLE tumors were previously reported to have high rates of C:G mutations (to A:T or T:A) asymmetrically introduced at cytosines replicated on the leading-strand template near three well-characterized origins of replication (Shinbrot et al., 2014). As a consequence, in these tumors we would expect to see predominantly C→A mutations in left-replicating regions and G→T in right-replicating regions, since we hypothesized these regions to be enriched for leading- and lagging-strand synthesis of the reference strand, respectively.

Indeed, when asymmetry is visualized along the chromosome, asymmetric C:G→A:T mutations, in a pooled cohort of 12 mutant-POLE colorectal and endometrial tumors, correspond strikingly to the slope of the replication timing profile (Figure 2). Higher densities of C→A mutations occur in regions of negative slope, while higher G→T densities occur in regions of positive slope. In TTRs (see Experimental Procedures), the magnitude and direction of this imbalance correlates well with the slope of the profile (R^2 = 0.53), while in constant-timing regions, no such correlation exists (R^2 = 0.08). Comparing left- and right-replicating regions, we measured a near 2-fold enrichment for the expected mutation type (Figure 1D). This is consistent with the recently reported preference for mutations at C:G base pairs where the cytosine is on the leading template strand measured next to three well-localized origins of replication (we will denote such base pairs C_{lft}:G_{rt}) (Shinbrot et al., 2014), and this validates our ability to extract replication direction from replication timing profiles. Furthermore, we tested our method on replication timing datasets from various cell types, including embryonic stem cells, induced pluripotent stem cells, neural precursor cells, and lymphoblast cell lines (Figure S2) (Ryba et al., 2010). All yielded very similar patterns of asymmetry, demonstrating the robustness of our method to tissue-specific variations in replication timing profiles.

Having analyzed each reference frame separately, we jointly considered transcriptional (T-class) and replicative (R-class) asymmetry. By focusing the analysis on regions that are both transcribed and located in TTRs, we can control for potential confounding factors such as chromatin state, since transcribed regions are typically in open chromatin and TTRs often reside at boundaries between open and closed chromatin (Lawrence et al., 2013). Surprisingly, we observed near-complete mutual exclusivity of R- and T-class asymmetries in the smoking-associated (lung) and POLE-associated (colorectal, endometrial) cohorts. In smoking-associated genomes, the direction of mutational asymmetries flips with transcription direction but shows little dependence on replication direction, even when controlling for transcription direction (Figure 1E). These observations show that smoking-associated lung cancers have a mutational pattern dominated by T-class asymmetry and with very little contribution from R-class asymmetry.

The opposite pattern was seen in POLE-associated cancers, in which mutational asymmetries depended entirely on replication direction and showed little response to change in transcription direction (Figure 1F). Thus, POLE-associated cancers have a mutational pattern dominated by R-class asymmetry and with almost zero T-class asymmetry.

The Asymmetry Map of Cancer Genomics

Having established that we can observe and separate transcriptional and replicative strand asymmetries for two well-understood mutational processes, we performed a comprehensive analysis of mutational strand asymmetries across many tumor types. We analyzed somatic mutations in 590 whole-genome sequences across 14 tumor types, partitioned into 18 patient cohorts (separating out POLE and microsatellite-instability [MSI] cases in the colorectal and endometrial cohorts and separating smokers from non-smokers in the two

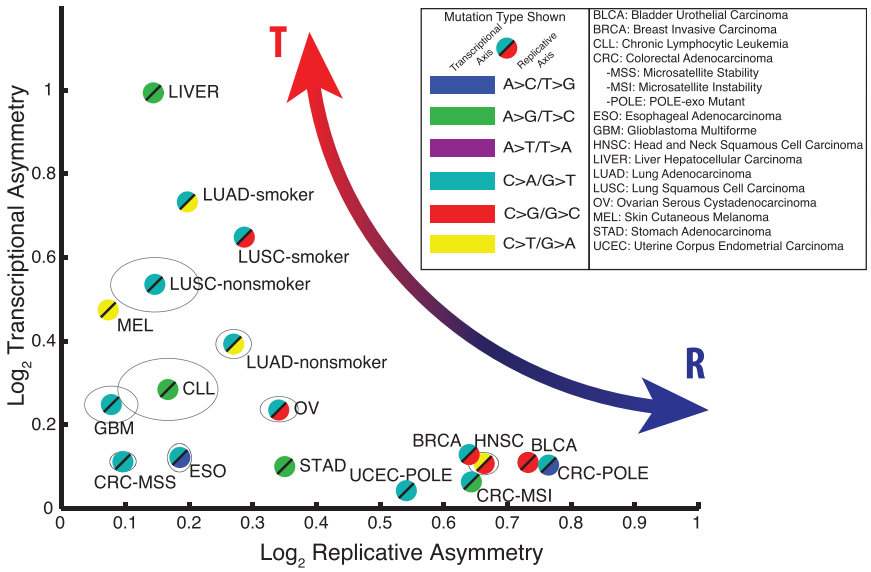

Figure 3. Cancer Cohorts Vary Widely across the Asymmetry Map

For each cohort listed, the maximal replicative asymmetry (x axis) and the maximal transcriptional asymmetry (y axis) were measured and plotted. Gray ellipses denote 95% confidence intervals for cohorts in which these extend beyond the bounds of the plot symbols.

lung cohorts; Table S1). For each cohort, we identified the mutation type having the largest asymmetry, with respect to transcription and to replication (Figure 3). This revealed a continuum of tumor types, ranging from tumors with predominant transcriptional (T-class) asymmetry to those with predominant replicative (R-class) asymmetry. For example, the melanoma, liver, and lung cohorts fell on the T-class side of the spectrum, while tumors frequently associated with an APOBEC signature (BLCA, BRCA, and HNSC) or MSI (CRC-MSI) showed R-class asymmetries at levels comparable to those of POLE tumors (CRC-POLE and UCEC-POLE).

The genomic asymmetry profiles of R-class tumors are strikingly concordant among each other within TTRs (POLE-APOBEC R^2 = 0.50, POLE-MSI R^2 = 0.66, APOBEC-MSI R^2 = 0.42) as well as with the slope of the replication timing profile (POLE R^2 = 0.56, APOBEC R^2 = 0.47, MSI R^2 = 0.49) (Figure 4), a trend robust to substituting replication timing profiles from various cell types (Ryba et al., 2010) (Figures S3 and S4). Importantly, we were able to detect statistically significant levels of asymmetry in all cohorts in at least one mutation type, and 8/15 showed either T-class or R-class asymmetry with greater than 50% enrichment (>0.58 in Figure 3) for at least one mutation type. Overall, these results demonstrate that mutational strand asymmetries are widespread across cancer.

Trends in Mutational Asymmetries

Next, we explored how mutational asymmetries depend on other variables such as expression levels, replication timing, and distance from transitions in replication or transcription direction. We focused on mutational processes that we identified as being the chief sources of asymmetry and identified the samples in which these processes were the major contributor to the overall mutational burden (Table S2). First, we analyzed transcriptional asymmetry as a function of gene expression level and replicative asymmetry as a function of DNA replication timing (Experimental Procedures). For most processes, we observed a decrease in mutational burden at higher expression levels (Figure 5A). Transcriptional asymmetry, which reflects TCR activity, was seen in a subset of these cohorts (liver A→G, smoking C→A, and UV C→T) and was maximal in highly expressed regions. In other cohorts (e.g., POLE C→A, microsatellite stable cancers [MSS] C→T), no transcriptional asymmetry was seen, perhaps due to the fact that other covariates (such as replication timing and chromatin state) correlate with expression levels but affect mutational burden via repair mechanisms that are independent of transcription. Similarly, for most processes, we observed a decrease in mutational burden in earliest-replicating regions (Figure 5B). Replicative asymmetry was seen in a subset of cohorts (MSI, APOBEC, POLE) and was strongest in earliest-replicating regions (especially in the case of POLE) but absent in other cohorts. To control for differences in chromatin state of TTRs and transcribed regions, in all of these cohorts we again performed a joint analysis of T- and R-class asymmetries (Figure S5).

We also analyzed the effect of genomic position with respect to transitions in transcription or replication direction. We examined transcriptional asymmetry around minus-to-plus transcription-direction transitions (Figure 5C), typically representing bidirectional promoters (Trinklein et al., 2004), and replicative asymmetry around left-to-right replication-direction transitions (Figure 5D), i.e., replication timing minima (Experimental Procedures). Mutations associated with smoking, UV, and liver cancer showed transcriptional strand asymmetries that flipped sign at transitions in transcription direction. Other cancers maintained balanced mutation densities on both sides of these transitions. Conversely, mutations associated with POLE, MSI, and APOBEC showed replicative strand asymmetries that flipped sign at replication timing minima. Other cohorts showed no such behavior at changes in replication direction. Exploring each of these asymmetries further can shed light on the operational mechanisms of mutagenesis and repair in these tumors.

Mutational Asymmetries Reveal Mechanisms of Mutagenesis

The above analyses led to insights into the mechanisms of incompletely understood mutational processes, such as the APOBEC and liver signatures. The APOBEC signature consists of C→G and C→T mutations in the context TCW (W = A or T) and is thought to reflect the activity of APOBEC-family cytidine

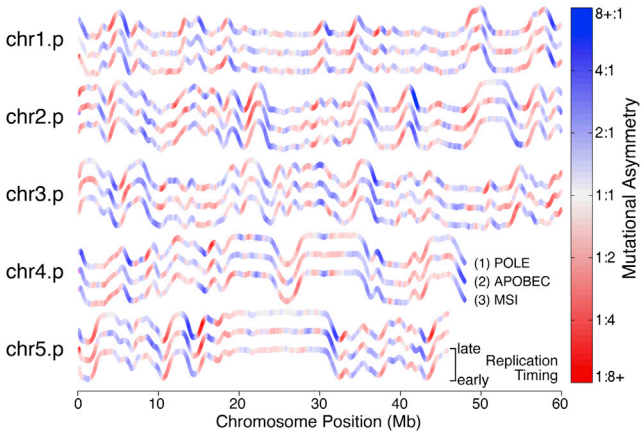

Figure 4. Replicative Asymmetry Is Concordant across Three Distinct R-Class Mutational Processes

Color representing mutational asymmetry is overlaid on replication timing profiles as in Figure 2. Profiles are shown in triplets colored by: (1) C→A:G→T asymmetry in 12 mutant-POLE colorectal and endometrial genomes, (2) G→C:C→G asymmetry in 22 APOBEC-enriched bladder, breast, and head-and-neck genomes, and (3) A→G:T→C asymmetry in 9 MSI-associated colon genomes.

deaminase enzymes (Alexandrov et al., 2013; Lawrence et al., 2013; Roberts et al., 2013). While the precise details of this phenomenon in cancer are not completely understood, a large body of work has characterized many aspects of this form of mutagenesis. APOBEC enzymes target ssDNA (Conticello, 2012), cause mutation clusters termed kataegis (Nik-Zainal et al., 2012a), and do not cause the usual increase in mutational densities in late-replicating, open-chromatin, and highly expressed regions (Kazanov et al., 2015). The main occurrences of ssDNA in human cells have been speculated to be at double-strand breaks (DSBs), R loops in transcription bubbles, and the lagging strand of the DNA replication fork. Experiments in model organisms have shown that APOBEC enzymes are indeed capable of inducing mutagenesis at DSBs (Taylor et al., 2013) and transcription bubbles (Lada et al., 2015; Taylor et al., 2014).

Our results suggest that, in humans, APOBEC mutagenesis primarily occurs on the lagging-strand template during DNA replication. The APOBEC signature shows strong R-class asymmetry, with a higher rate of C→G and C→T mutations in right-replicating regions (Figures 3 and 5), where reference-strand DNA is predicted to be replicated as the lagging-strand template, exposed as ssDNA between Okazaki segments. The magnitude of this asymmetry increases with enrichment of the APOBEC signature (Figure 6A), and joint analysis of both classes of asymmetry placed APOBEC squarely at the R-class end of the spectrum (Figure 6B). Note that, in all breast, bladder, and head and neck samples, even when the fraction of APOBEC mutations is low, significant R-class asymmetry is observed, suggesting that it is not merely a property of hypermutation. These findings are further supported by research in model organisms concurrent with this study. Bhagwat et al. (2016) found that overexpression of APOBEC3G in *E. coli* leads to a C:G→T:A signature that shows a replicative strand bias consistent with cytosine deamination of the lagging-strand template. Additionally, in a yeast model, Roberts and colleagues (Hoopes et al., 2016) showed that overexpression of APOBEC3A and B produces a similar replicative asymmetry.

Taken together, these findings suggest that the R-class model is the primary mechanism for APOBEC mutagenesis in humans. In this model, APOBEC-family enzymes deaminate cytosines on the lagging-strand template during DNA replication, likely while it is single stranded (Figure 6C). The resulting uracil is excised, and subsequent replication either incorporates an adenine across from this abasic site, resulting in a C→T mutation, or (mediated by REV1 activity) incorporates a cytosine, resulting in a C→G mutation (Helleday et al., 2014). This model is also supported by the unusual lack of increase in mutational densities in late-replicating regions (Figure 5) (Kazanov et al., 2015). As MMR has been suggested to underlie this variation in mutational densities (Supek and Lehner, 2015), this may imply that APOBEC-associated mutagenesis evades the MMR machinery. This is consistent with the R-class model, in which the lagging-strand template (i.e., the parental strand) is deaminated; MMR, which relies on the parental strand to correct mistakes on the nascent strand, would be unable to correct this error without a correct template. Genome-wide, we observed only a small amount of APOBEC T-class asymmetry (Figure 6C), but a previous report showed that overexpressing APOBEC in yeast resulted in mutations that were transcriptionally asymmetric (Lada et al., 2015). Indeed, when we restricted to 5′ UTRs (the regions reported to have the strongest transcriptional asymmetry), we revealed APOBEC T-class asymmetry also in humans (Figure S6). However, in the genome-wide analysis, the T-class asymmetry is dwarfed by the contributions from the R-class model.

Intriguingly, we observed a similar APOBEC mutational R-class asymmetry in the human germline. We measured replicative asymmetry in a set of 11,020 de novo germline mutations (Francioli et al., 2015) and found that C→G and C→T mutations showed no significant R-class asymmetry outside of the TCW context (1127 C→G/T versus 1171 G→A/C, in the leading-strand reference frame, $p = 0.35$). When we focused on the TCW context (the preferred target of APOBEC mutagenesis), we were able to detect a significant level of R-class asymmetry (109 TCW→G/T versus 151 WGA→A/C mutations, in the leading-strand reference frame, $p = 0.014$; Figure S7). Further studies analyzing a larger number of mutations will be required to fully understand the potential impact of APOBEC enzymes on germline mutagenesis and its evolutionary implications.

A Mechanism of Transcription-Coupled DNA Damage

In contrast to APOBEC- and MSI-associated mutations, liver A:T→G:C mutations showed little replicative asymmetry but instead showed transcriptional asymmetry similar to that seen in lung cancer (LUSC and LUAD in Figure 3; smoking C→A versus G→T in Figure 5). Closer inspection of transcriptional strand asymmetry revealed a distinction between the liver A→G signature and the two other T-class examples: UV-associated C→T and smoking-associated G→T. Mutations generated by UV light and smoking are lower in density on the transcribed

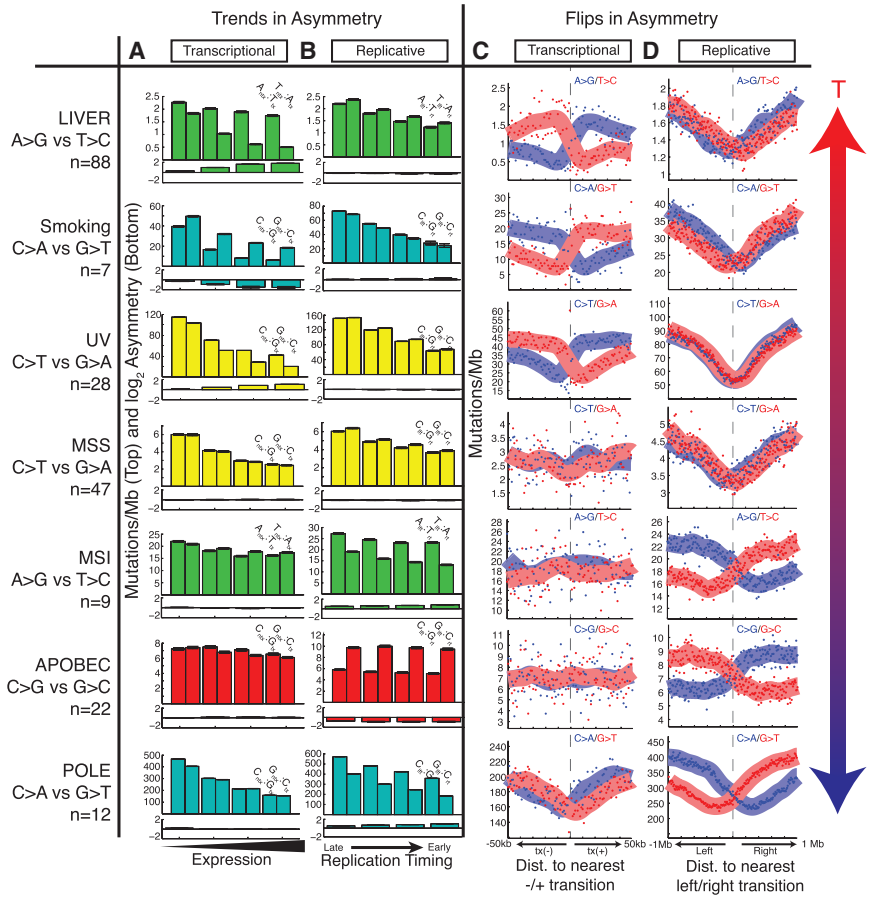

Figure 5. Trends and Flips in Asymmetry

(A) Transcriptional strand asymmetry measured across four quartiles of expression levels. Total mutation density tends to decrease with expression level, and T-class asymmetry (liver, smoking, UV) is maximal at highest expression.

(B) Replicative strand asymmetry measured across four quartiles of replication timing. Total mutational density tends to decrease with earlier replication, and R-class asymmetry (MSI, APOBEC, POLE) is maximal at earliest replication.

(C) Strand-specific mutational density measured in the vicinity of bidirectional promoters. T-class asymmetry flips at transitions from tx(−) to tx(+) regions.

(D) Strand-specific mutational density measured in the vicinity of replication timing minima. R-class asymmetry flips at these left-to-right transitions.

Error bars represent 95% confidence intervals.

strand compared to proximal IGR (due to TCR), while mutational densities on the non-transcribed strand remain constant regardless of transcription (Figure 7A). The liver A→G signature also shows the expected TCR effect on the transcribed strand; however, mutational densities of A→G on the non-transcribed strand drastically *increase* in transcribed regions. This suggests that transcriptional asymmetry in liver is not only due to repair of the transcribed strand but is also compounded by damage to the complementary non-transcribed strand, a phenomenon we call transcription-coupled damage (TCD).

At the extreme, we observed one liver cancer sample, HX17T, which showed a 3-fold transcription-dependent increase in A→G mutational densities on the non-transcribed strand (Figure 7B). This is in contrast to the usual trend in which non-transcribed strand mutational densities decrease with expression due to more effective global genome repair (GGR) and MMR in open-chromatin and early-replicating regions. This effect is unique to the A→G signature. In that same sample, C→A mutational densities (driven by carcinogen attack ;Alexandrov et al., 2013) showed the usual decrease on both strands (Figure 7C). In our cohort of 88 liver cancer samples, we examined the slope of this response of mutational density to expression level for each of the 12 possible mutation types (Figure 7D). In a two-tailed test, we found that 25/88 of the liver patients showed a significant increase in A→G mutational densities on the non-transcribed strand (Experimental Procedures), while only 9/88 showed a significant decrease, showing that, in the majority of samples, the A→G signature does not show the usual repair (Table S3). As mentioned before, the contributions of MMR and GGR are confounding factors when considering the effect of expression levels on mutational densities, since higher expression is correlated with earlier replication timing and a more open chromatin state. As a result, on the non-transcribed strand, higher expression could lead to both increased damage by TCD and higher levels of repair by MMR and GGR. Different contributions of these damage and repair processes likely underlie the variation that we observed across patients.

While the strong transcriptional asymmetry of the A→G signature in liver cancer has been noted (Alexandrov et al., 2013), we propose that this is due to two separate processes operating on different strands—TCD and TCR (Figure 7E). This explains the extreme transcriptional asymmetry of liver A→G compared to other signatures (Figure 3). Furthermore these results suggest that the A→G signature is caused by a mutational process distinct from typical bulky-adduct damage. Finally, we noticed that one colorectal patient (“CRC-8”) from an earlier study of nine colorectal whole genomes (Bass et al., 2011) showed the same signature of TCD. Thus, this phenomenon may be enriched in liver but not exclusive to it.

Mismatch Repair Balances Mutational Asymmetry

Colorectal cancers with functional MMR (i.e., MSS) show little replicative asymmetry of any mutation type (aside from C→G mutations, which are in part due to low levels of APOBEC signature). As mentioned above, loss of functional polymerase ε proofreading results in R-class asymmetry. MSI colorectal tumors, typically resulting from damage to the MMR system (Kane et al., 1997; Shinbrot et al., 2014; Vilar and Gruber, 2010), also

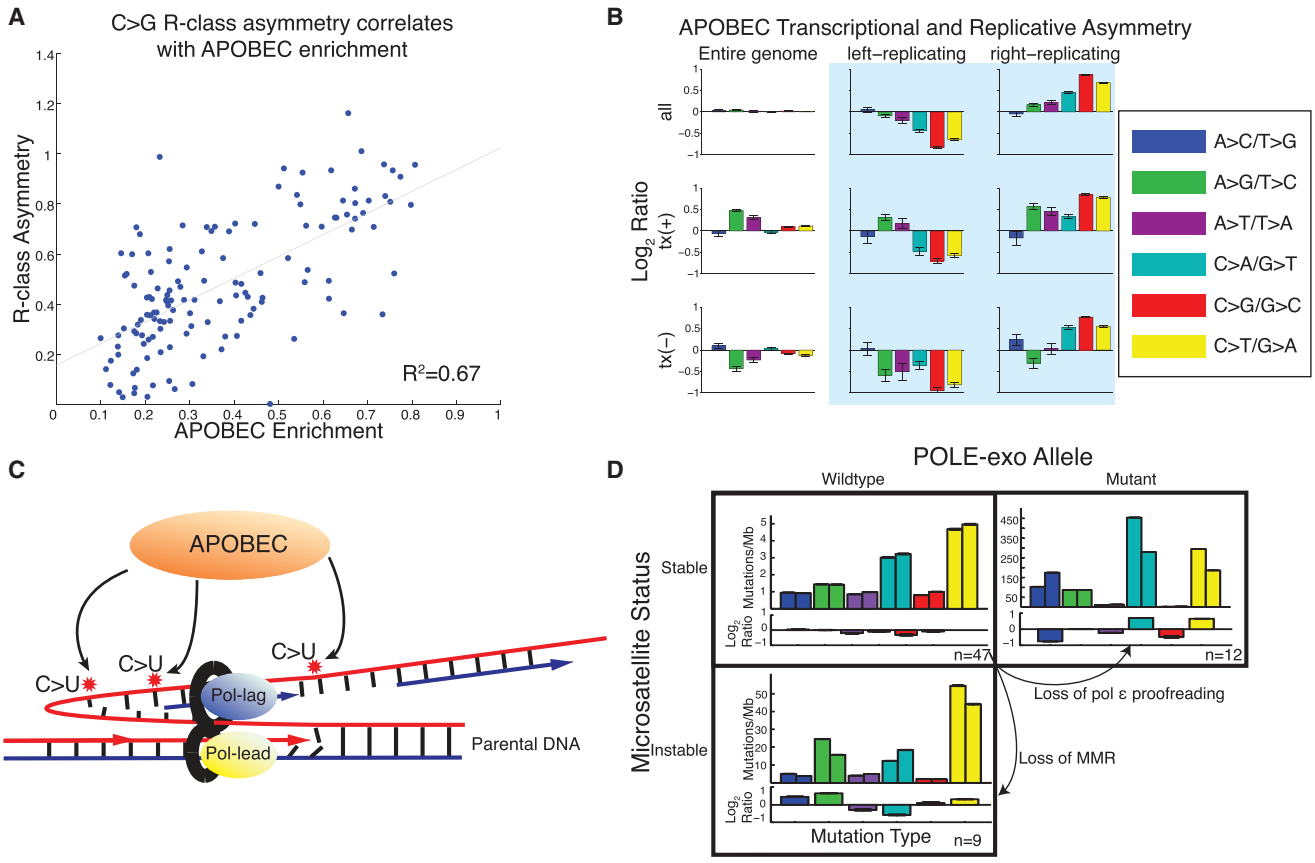

Figure 6. R-Class Asymmetries Associated with APOBEC and MSI

(A) Bladder, breast, and head-and-neck cohorts. Samples with highest enrichment of APOBEC signature show highest replicative asymmetry of C→G mutations.

(B) APOBEC-enriched samples are dominated by replicative asymmetry (as in Figures 1E and 1F)

(C) Proposed model: APOBEC deaminates cytosine to uracil on the ssDNA of the lagging-strand template during DNA replication.

(D) R-class asymmetry in MSS, MSI, and POLE mutant cohorts. MSS samples have little asymmetry. Loss of MMR or pol ε proofreading leads to imbalance in mutations between the leading and lagging strands.

Error bars represent 95% confidence interval.

show replicative asymmetry (Figure 6D). This would suggest that MMR (in addition to exonuclease proofreading) is required to balance mutational asymmetries generated during DNA replication. This phenomenon has also been reported in yeast (Lujan et al., 2012), and our results suggest that the same is true in humans.

The implications of this role for MMR reach beyond the realm of cancer research. Without such balancing, asymmetric introduction of germline mutations would result in local depletion of specific nucleotides over evolution. Indeed, a slight replicative imbalance can be detected in the reference genome: C_{lft}:G_{rt} base pairs outnumber G_{lft}:C_{rt} base pairs by 2.1% on average, and A_{lft}:T_{rt} base pairs outnumber T_{lft}:A_{rt} base pairs by 3.7%. This is in line with a previous result measuring a mean compositional skew of 3.72% (Chen et al., 2011). However, the relative mildness of these imbalances, compared to the much stronger mutational asymmetries seen in MMR-deficient tumors, suggests that MMR has played an important role throughout evolution in maintaining genome symmetry.

DISCUSSION

Our results highlight the widespread mutational strand asymmetries observed in cancer genomes, mediated by DNA replication, RNA transcription, and their associated repair pathways. Study of these prominent sources of asymmetry has mostly been performed in model organisms (Lobry, 1996; Lujan et al., 2012; McLean et al., 1998; Pavlov et al., 2002; Touchon et al., 2005), and here, we extend this analysis to humans via cancer genomics. Our work addresses several of the most prominent processes in cancer and provides insight into their biological mechanisms. Analysis of asymmetries associated with the growing number of mutational processes discovered by sophisticated signature decoupling approaches (Alexandrov et al., 2013; Kasar et al., 2015; Lawrence et al., 2013) will provide a deeper view of these processes and will further illuminate their underlying sources. Our ability to detect mutational asymmetries will improve with higher-resolution replication timing and transcription maps and with improving knowledge of human replication origins. Finally, we note that there may

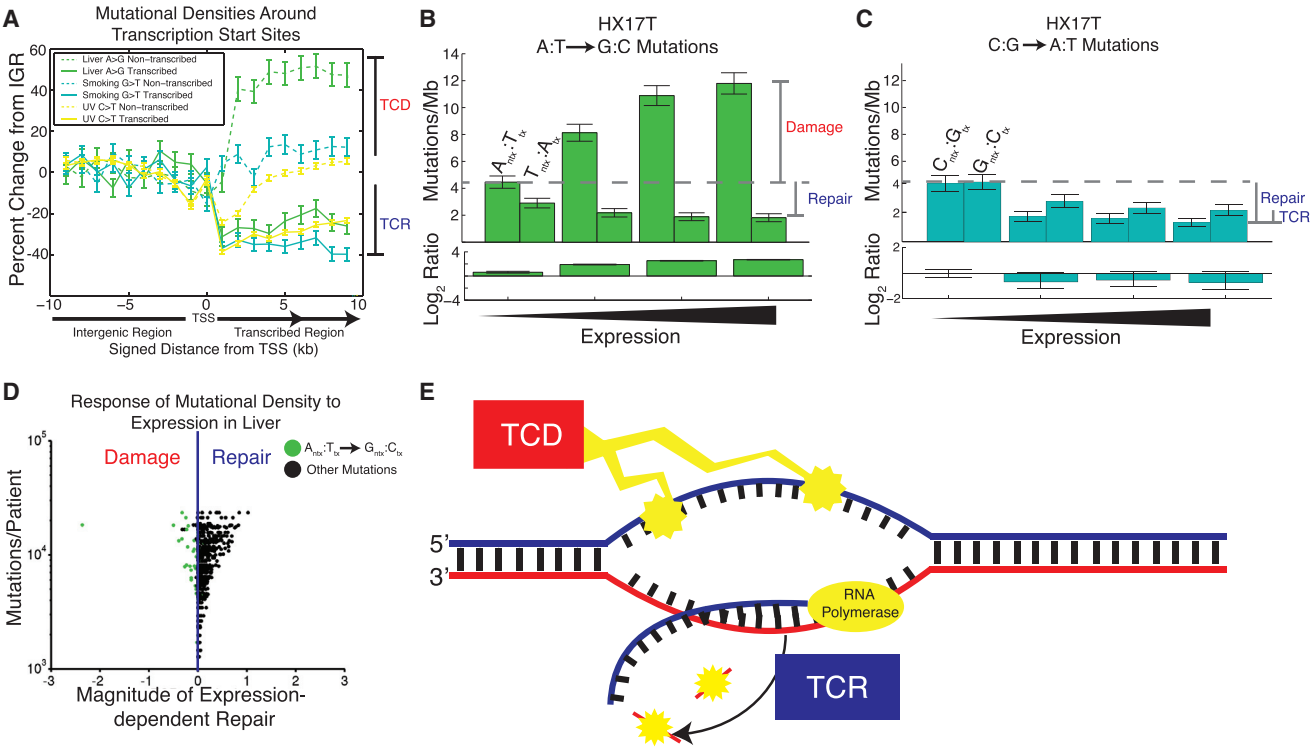

Figure 7. Transcription-Coupled Damage in Liver Cancer

(A) Mutational densities in the vicinity of promoters. When crossing from non-transcribed intergenic regions (IGR) to transcribed regions, mutational densities on the transcribed strand fall, reflecting TCR. On the non-transcribed strand there is usually little change from IGR levels, with the notable exception of liver cancer, in which mutational densities increase from IGR levels, consistent with transcription-coupled damage (TCD).

(B) Liver cancer patient HX17T shows a dramatic expression-dependent increase in A→G mutational densities on the non-transcribed strand only.

(C) In the same patient, G→T mutational densities show only the usual expression-dependent decrease on both strands.

(D) Most liver patients show dominant TCR. However, for A→G mutations on the non-transcribed strand (green dots), some show the opposite trend, reflecting dominant TCD. The leftmost dot is patient HX17T.

(E) TCD damages the non-transcribed strand, exposed as ssDNA during transcription. TCR repairs the transcribed strand. Both of these processes contribute to T-class asymmetry.

Error bars represent 95% confidence interval.

be additional useful reference frames for symmetry breaking beyond the two used here.

Classifying patients according to their patterns of mutational strand asymmetry may have clinical relevance. Tumors with defects in DNA repair mechanisms have been shown to be vulnerable to synthetically lethal therapeutic interventions that further disrupt genome stability (Carreras Puigvert et al., 2015; Curtin, 2012; Middleton et al., 2015). As discussed, R-class asymmetries can be introduced either by asymmetric damage at the replication fork or by deficiency in the proof-reading and repair of DNA synthesis. In the latter case, R-class asymmetry may serve as a proxy for replicative stress and could suggest synthetic lethality as an effective avenue for treatment. Similarly, individual patients of T-class tumor types (such as melanoma) that do not themselves exhibit T-class asymmetry potentially reveal a deficiency of TCR. Thus, analyzing asymmetries of both classes may facilitate a better match between patients and treatments.

Additionally, patient-specific responses to classic chemotherapy drugs are often poorly understood and are difficult to predict. Analyzing responses to these drugs in conjunction with mutation rates and asymmetries at the replication fork or transcription bubble may provide useful insights into these drugs' functionality. This, in turn, could allow for more targeted use of the drugs, as well as better control of unintended side effects.

Strand asymmetry may be particularly impactful in the earliest driving events of cancer, due to that defining feature of carcinogenesis, the transformation of cells into an aberrantly proliferative state. A particular DNA lesion may push the cell from a resting state (without DNA replication) into active mitosis, and the initial strand hit by that driver lesion is crucial; due to absent (or infrequent DNA) replication in these pre-malignant cells, DNA damage of the non-transcribed strand may wait a very long time to be propagated as a mutation to the transcribed strand where it can exert its driving effect. We also note that the strand asymmetries we observe in cancer may inform the debate on the "immortal DNA strand hypothesis" and its possible relevance to cancer (Cairns, 2006; Yadlapalli and Yamashita, 2013; Tomasetti and Bozic, 2015).

Beyond cancer, somatic mutational processes play an important role in a broad range of diseases, including aging (Kennedy et al., 2012; Kenyon, 2010), autoimmune disease (Ross, 2014), and neurological disorders (Poduri et al., 2013). Many of the same background mutational processes are active in cancerous and non-cancerous cells (such as methylated CpG deamination/"aging," UV damage, and environmental mutagens), and the lessons learned from the clonal expansion of mutations in cancer will aid in the understanding of these universal processes. Novel mutational and repair processes continue to emerge from cancer genome sequencing studies, and viewing them through the lens of mutational strand asymmetry can provide immediate insights into their molecular mechanisms.

EXPERIMENTAL PROCEDURES

Data Provenance

We assembled a collection of 590 whole-genome sequences from 14 tumor types by combining published data from the Cancer Genome Atlas (TCGA; dbGAP: phs000178.v1.p1) with other published datasets (Alexandrov et al., 2013; Dulak et al., 2013; Lawrence et al., 2014; Bass et al., 2011; Berger et al., 2012; Wang et al., 2011).

Statistical Analysis

MATLAB code to generate asymmetry metrics and figures is available at www.broadinstitute.org/cancer/cga/AsymTools.

Determining Transcription and Replication Direction and Calculating Densities

Transcription direction was determined according to the Refseq database. Replication direction was defined using replication timing profiles generated in six lymphoblastoid cell lines, as published in Koren et al. (2012). We determined left- and right-replicating regions based on the sign of the derivative of the profile (negative is left-replicating and positive is right-replicating). To only define regions in TTRs, we required a slope with a magnitude of at least 250 replication timing units ("rtu") per Mb. These arbitrary units range from 100 to 1,200, denoting the beginning and end of S phase.

Mutational densities for a given base pair change $b1{:}b2 \rightarrow m_1{:}m_2$ and its complementary mutation $b2{:}b1 \rightarrow m_2{:}m_1$ in a given list of regions were determined by the formula:

$$r_{b1:b2\rightarrow m1:m2} = \frac{n_{b1\rightarrow m1}}{p * N_{b1}}$$

$$r_{b2:b1\rightarrow m2:m1} = \frac{n_{b2\rightarrow m2}}{p * N_{b2}}$$

where $n_{b\rightarrow m}$ is the number of observations of $b\rightarrow m$ mutations with respect to the genomic reference strand, N_b is the number of chances for this mutation to happen, i.e., the number of occurrences of the motif b in the given region of the reference genome (on the genomic reference strand), and p is the number of patients analyzed. Asymmetry was then calculated in a given region by:

$$a_{b\rightarrow m} = log_2\left(\frac{r_{b1:b2\rightarrow m1:m2}}{r_{b2:b1\rightarrow m2:m1}}\right)$$

as seen in Figure 1.

Calculating Global Mutational Asymmetries

When calculating global mutational asymmetries, redundant mutations with respect to a given strand are summed together. For example, to calculate global genome mutational densities with respect to the leading strand, we calculate:

$$r_{b1:b2\rightarrow m1:m2} = \frac{n_{l,b1\rightarrow m1} + n_{r,b2\rightarrow m2}}{p * (N_{l,b1} + N_{r,b2})}$$

$$r_{b2:b1\rightarrow m2:m1} = \frac{n_{l,b2\rightarrow m2} + n_{r,b1\rightarrow m1}}{p * (N_{l,b2} + N_{r,b1})}$$

$$a_{b\rightarrow m} = log_2\left(\frac{r_{b1:b2\rightarrow m1:m2}}{r_{b2:b1\rightarrow m2:m1}}\right)$$

where subscripts "l" and "r" refer to events in left- and right-replicating regions, respectively. Essentially, this approach distinguishes a $b_1{:}b_2$ base pair by whether base b_1 is on the presumed leading/lagging strand rather than the genomic reference. The same approach is used for calculating asymmetry with respect to the sense strand, using tx(+) and tx(−) regions instead of left- and right-replicating, respectively.

Correlation of R-Class Asymmetry with Direction of TTRs

Replication timing data and POLE, APOBEC, and MSI asymmetry metrics were aggregated in 100 kb bins and smoothed using a moving average over 10 bins. The replication timing data were plotted, and the profiles were colored by the asymmetry metrics in the POLE cohort (Figure 2) or all three R-class cohorts (Figure 4). Correlations restricted to TTRs were calculated by only considering regions with a slope of >250 rtu/Mb.

Binning by Expression and Replication Timing

Expression profiles were an average of many cell lines, as used in Lawrence et al., (2013). To perform binning by functional covariates as seen in Figures 5A and 5B, expression and replication timing values were projected onto 20 kb intervals. These intervals were then sorted by expression for Figure 5A and replication timing for Figure 5B and separated into bins with an even number of intervals, and mutational rates and asymmetry were calculated for the intervals in each bin.

Identifying Transcription and Replication Direction Transitions

Minus-to-plus transcription transitions were identified by taking all bidirectional gene pairs (opposing genes with transcription start sites within 1 kb of each other ; Trinklein et al., 2004) in the Refseq database and calculating the midpoint of their transcription start sites. Left-to-right replication transitions were similarly identified by calculating the midpoint between the right and left boundaries of defined left- and right-replicating regions, respectively.

Determining Response of Mutational Densities to Increasing Expression

Response of mutational densities to increasing expression, as shown in Figures 7B and 7C, was performed for each patient and for each of the six possible mutations, creating a figure as shown in Figure 7D. Then linear regression was performed separately on each series of bars (the left bars for the non-transcribed strand and the right bars for the transcribed strand). For these two regressions, we calculated a 95% confidence interval for the slope and assessed significance based on whether zero fell inside of the interval. Then for each regression, we plotted the more conservative bound of the corresponding confidence interval, i.e., the value closer to or equal to zero.

Creating a Hypothetical Replication Timing Distribution

The hypothetical replication timing curve shown in Figure S1A was created by first taking its real counterpart in Figure S1B. Then the locations of origins of replication were randomly assigned, assuming a density of one origin per 40 kb. From these origins, a more detailed profile was drawn by assuming constant polymerase speed and smoothing the result.

SUPPLEMENTAL INFORMATION

Supplemental Information includes seven figures and three tables and can be found with this article online at http://dx.doi.org/10.1016/j.cell.2015.12.050.

AUTHOR CONTRIBUTIONS

Conceptualization, M.S.L., P.P., G.G., N.J.H., P.S., D.A.W., E.S., K.R.C., A. Koren, and J.K.; Methodology, M.S.L., P.P., N.J.H., and P.S.; Software, N.J.H. and M.S.L.; Formal Analysis, N.J.H., M.S.L., and P.P.; Investigation, N.J.H., P.P., and M.S.L.; Resources, M.S.L., G.G., A. Koren, and D.A.W.; Data Curation, E.R., N.J.H., P.P., M.S.L., and A. Koren; Writing – Original Draft, N.J.H., M.S.L., A. Koren, P.P., and G.G.; Writing – Review & Editing, N.J.H., M.S.L., A. Koren, P.P., G.G., D.A.W., P.C.H., E.S., K.R.C., E.R., J.M.H., P.S., Y.E.M., A. Kamburov, and L.Z.B.; Visualization, N.J.H. and M.S.L.; Supervision, G.G., M.S.L., P.P., A. Koren, D.A.W., and P.C.H.

ACKNOWLEDGMENTS

We thank Ashok Bhagwat and Steven Roberts and their collaborators for sharing their unpublished data with us and allowing us to reference them in this work. We thank John Iafrate for valuable insights about the relevance of strand asymmetry in carcinogenesis. G.G. was partially funded by the Paul C. Zamecnik, MD, Chair in Oncology at Massachusetts General Hospital. G.G. and M.S.L. were partially funded by the NIH TCGA Genome Data Analysis Center (U24CA143845). M.S.L. was partially funded by the NHGRI Genome Sequencing Center (U54HG003067). E.S., K.R.C., and D.A.W. were partially funded by NHGRI grant (U54HG003273). N.J.H., P.P., Y.E.M., and A. Kamburov were funded by G.G.'s startup funds at MGH.

Received: November 13, 2015
Revised: December 21, 2015
Accepted: December 24, 2015
Published: January 21, 2016

REFERENCES

Alexandrov, L.B., Nik-Zainal, S., Wedge, D.C., Aparicio, S.A., Behjati, S., Biankin, A.V., Bignell, G.R., Bolli, N., Borg, A., Børresen-Dale, A.L., et al.; Australian Pancreatic Cancer Genome Initiative; ICGC Breast Cancer Consortium; ICGC MMML-Seq Consortium; ICGC PedBrain (2013). Signatures of mutational processes in human cancer. Nature *500*, 415–421.

Bass, A.J., Lawrence, M.S., Brace, L.E., Ramos, A.H., Drier, Y., Cibulskis, K., Sougnez, C., Voet, D., Saksena, G., Sivachenko, A., et al. (2011). Genomic sequencing of colorectal adenocarcinomas identifies a recurrent VTI1A-TCF7L2 fusion. Nat. Genet. *43*, 964–968.

Berger, M.F., Hodis, E., Heffernan, T.P., Deribe, Y.L., Lawrence, M.S., Protopopov, A., Ivanova, E., Watson, I.R., Nickerson, E., Ghosh, P., et al. (2012). Melanoma genome sequencing reveals frequent PREX2 mutations. Nature *485*, 502–506.

Bhagwat, A.S., Hao, W., Townes, J.P., Lee, H., Tang, H., and Foster, P.L. (2016). Strand-biased Cytosine deamination at the Replication Fork causes Cytosine to Thymine Mutations in Escherichia coli. Proc. Natl. Acad. Sci. USA. http://dx.doi.org/10.1073/pnas.1522325113.

Cairns, J. (2006). Cancer and the immortal strand hypothesis. Genetics *174*, 1069–1072.

Carreras Puigvert, J., Sanjiv, K., and Helleday, T. (2015). Targeting DNA repair, DNA metabolism and replication stress as anti-cancer strategies. FEBS J. Published online October 28, 2015. http://dx.doi.org/10.1111/febs.13574.

Chapman, M.A., Lawrence, M.S., Keats, J.J., Cibulskis, K., Sougnez, C., Schinzel, A.C., Harview, C.L., Brunet, J.P., Ahmann, G.J., Adli, M., et al. (2011). Initial genome sequencing and analysis of multiple myeloma. Nature *471*, 467–472.

Chen, C.L., Duquenne, L., Audit, B., Guilbaud, G., Rappailles, A., Baker, A., Huvet, M., d'Aubenton-Carafa, Y., Hyrien, O., Arneodo, A., and Thermes, C. (2011). Replication-associated mutational asymmetry in the human genome. Mol. Biol. Evol. *28*, 2327–2337.

Conticello, S.G. (2012). Creative deaminases, self-inflicted damage, and genome evolution. Ann. N Y Acad. Sci. *1267*, 79–85.

Curtin, N.J. (2012). DNA repair dysregulation from cancer driver to therapeutic target. Nat. Rev. Cancer *12*, 801–817.

Denissenko, M.F., Pao, A., Tang, M., and Pfeifer, G.P. (1996). Preferential formation of benzo[a]pyrene adducts at lung cancer mutational hotspots in P53. Science *274*, 430–432.

Donahue, B.A., Yin, S., Taylor, J.S., Reines, D., and Hanawalt, P.C. (1994). Transcript cleavage by RNA polymerase II arrested by a cyclobutane pyrimidine dimer in the DNA template. Proc. Natl. Acad. Sci. USA *91*, 8502–8506.

Dulak, A.M., Stojanov, P., Peng, S., Lawrence, M.S., Fox, C., Stewart, C., Bandla, S., Imamura, Y., Schumacher, S.E., Shefler, E., et al. (2013). Exome and whole-genome sequencing of esophageal adenocarcinoma identifies recurrent driver events and mutational complexity. Nat. Genet. *45*, 478–486.

Fousteri, M., and Mullenders, L.H. (2008). Transcription-coupled nucleotide excision repair in mammalian cells: molecular mechanisms and biological effects. Cell Res. *18*, 73–84.

Francioli, L.C., Polak, P.P., Koren, A., Menelaou, A., Chun, S., Renkens, I., van Duijn, C.M., Swertz, M., Wijmenga, C., van Ommen, G., et al.; Genome of the Netherlands Consortium (2015). Genome-wide patterns and properties of de novo mutations in humans. Nat. Genet. *47*, 822–826.

Green, P., Ewing, B., Miller, W., Thomas, P.J., and Green, E.D.; NISC Comparative Sequencing Program (2003). Transcription-associated mutational asymmetry in mammalian evolution. Nat. Genet. *33*, 514–517.

Guilbaud, G., Rappailles, A., Baker, A., Chen, C.L., Arneodo, A., Goldar, A., d'Aubenton-Carafa, Y., Thermes, C., Audit, B., and Hyrien, O. (2011). Evidence for sequential and increasing activation of replication origins along replication timing gradients in the human genome. PLoS Comput. Biol. *7*, e1002322.

Hanawalt, P.C., and Spivak, G. (2008). Transcription-coupled DNA repair: two decades of progress and surprises. Nat. Rev. Mol. Cell Biol. *9*, 958–970.

Helleday, T., Eshtad, S., and Nik-Zainal, S. (2014). Mechanisms underlying mutational signatures in human cancers. Nat. Rev. Genet. *15*, 585–598.

Hoopes, J., Cortez, L., Mertz, T., Malc, E.P., Mieczkowski, P.A., and Roberts, S.A. (2016). APOBEC3A and APOBEC3B Deaminate the Lagging Strand Template during DNA Replication. Cell Reports. Published online January 28, 2016. http://dx.doi.org/10.1016/j.celrep.2016.01.021.

Jiang, G., and Sancar, A. (2006). Recruitment of DNA damage checkpoint proteins to damage in transcribed and nontranscribed sequences. Mol. Cell. Biol. *26*, 39–49.

Jinks-Robertson, S., and Bhagwat, A.S. (2014). Transcription-associated mutagenesis. Annu. Rev. Genet. *48*, 341–359.

Johnson, R.E., Klassen, R., Prakash, L., and Prakash, S. (2015). A Major Role of DNA Polymerase δ in Replication of Both the Leading and Lagging DNA Strands. Mol. Cell *59*, 163–175.

Kane, M.F., Loda, M., Gaida, G.M., Lipman, J., Mishra, R., Goldman, H., Jessup, J.M., and Kolodner, R. (1997). Methylation of the hMLH1 promoter correlates with lack of expression of hMLH1 in sporadic colon tumors and mismatch repair-defective human tumor cell lines. Cancer Res. *57*, 808–811.

Kasar, S., Kim, J., Improgo, R., Tiao, G., Polak, P., Haradhvala, N., Lawrence, M.S., Kiezun, A., Fernandes, S.M., Bahl, S., et al. (2015). Whole-genome sequencing reveals activation-induced cytidine deaminase signatures during indolent chronic lymphocytic leukaemia evolution. Nat. Commun. *6*, 8866.

Kazanov, M.D., Roberts, S.A., Polak, P., Stamatoyannopoulos, J., Klimczak, L.J., Gordenin, D.A., and Sunyaev, S.R. (2015). APOBEC-Induced Cancer Mutations Are Uniquely Enriched in Early-Replicating, Gene-Dense, and Active Chromatin Regions. Cell Rep. *13*, 1103–1109.

Kennedy, S.R., Loeb, L.A., and Herr, A.J. (2012). Somatic mutations in aging, cancer and neurodegeneration. Mech. Ageing Dev. *133*, 118–126.

Kenyon, C.J. (2010). The genetics of ageing. Nature *464*, 504–512.

Koren, A., Tsai, H.J., Tirosh, I., Burrack, L.S., Barkai, N., and Berman, J. (2010). Epigenetically-inherited centromere and neocentromere DNA replicates earliest in S-phase. PLoS Genet. *6*, e1001068.

Koren, A., Polak, P., Nemesh, J., Michaelson, J.J., Sebat, J., Sunyaev, S.R., and McCarroll, S.A. (2012). Differential relationship of DNA replication timing

to different forms of human mutation and variation. Am. J. Hum. Genet. *91*, 1033–1040.

Lada, A.G., Kliver, S.F., Dhar, A., Polev, D.E., Masharsky, A.E., Rogozin, I.B., and Pavlov, Y.I. (2015). Disruption of Transcriptional Coactivator Sub1 Leads to Genome-Wide Re-distribution of Clustered Mutations Induced by APOBEC in Active Yeast Genes. PLoS Genet. *11*, e1005217.

Lawrence, M.S., Stojanov, P., Polak, P., Kryukov, G.V., Cibulskis, K., Sivachenko, A., Carter, S.L., Stewart, C., Mermel, C.H., Roberts, S.A., et al. (2013). Mutational heterogeneity in cancer and the search for new cancer-associated genes. Nature *499*, 214–218.

Lawrence, M.S., Stojanov, P., Mermel, C.H., Robinson, J.T., Garraway, L.A., Golub, T.R., Meyerson, M., Gabriel, S.B., Lander, E.S., and Getz, G. (2014). Discovery and saturation analysis of cancer genes across 21 tumour types. Nature *505*, 495–501.

Lobry, J.R. (1996). Asymmetric substitution patterns in the two DNA strands of bacteria. Mol. Biol. Evol. *13*, 660–665.

Lujan, S.A., Williams, J.S., Pursell, Z.F., Abdulovic-Cui, A.A., Clark, A.B., Nick McElhinny, S.A., and Kunkel, T.A. (2012). Mismatch repair balances leading and lagging strand DNA replication fidelity. PLoS Genet. *8*, e1003016.

McLean, M.J., Wolfe, K.H., and Devine, K.M. (1998). Base composition skews, replication orientation, and gene orientation in 12 prokaryote genomes. J. Mol. Evol. *47*, 691–696.

Mellon, I., Spivak, G., and Hanawalt, P.C. (1987). Selective removal of transcription-blocking DNA damage from the transcribed strand of the mammalian DHFR gene. Cell *51*, 241–249.

Middleton, F.K., Patterson, M.J., Elstob, C.J., Fordham, S., Herriott, A., Wade, M.A., McCormick, A., Edmondson, R., May, F.E., Allan, J.M., et al. (2015). Common cancer-associated imbalances in the DNA damage response confer sensitivity to single agent ATR inhibition. Oncotarget *6*, 32396–32409.

Miyabe, I., Kunkel, T.A., and Carr, A.M. (2011). The major roles of DNA polymerases epsilon and delta at the eukaryotic replication fork are evolutionarily conserved. PLoS Genet. *7*, e1002407.

Nick McElhinny, S.A., Gordenin, D.A., Stith, C.M., Burgers, P.M., and Kunkel, T.A. (2008). Division of labor at the eukaryotic replication fork. Mol. Cell *30*, 137–144.

Nik-Zainal, S., Alexandrov, L.B., Wedge, D.C., Van Loo, P., Greenman, C.D., Raine, K., Jones, D., Hinton, J., Marshall, J., Stebbings, L.A., et al.; Breast Cancer Working Group of the International Cancer Genome Consortium (2012a). Mutational processes molding the genomes of 21 breast cancers. Cell *149*, 979–993.

Nik-Zainal, S., Van Loo, P., Wedge, D.C., Alexandrov, L.B., Greenman, C.D., Lau, K.W., Raine, K., Jones, D., Marshall, J., Ramakrishna, M., et al.; Breast Cancer Working Group of the International Cancer Genome Consortium (2012b). The life history of 21 breast cancers. Cell *149*, 994–1007.

Pavlov, Y.I., Newlon, C.S., and Kunkel, T.A. (2002). Yeast origins establish a strand bias for replicational mutagenesis. Mol. Cell *10*, 207–213.

Pleasance, E.D., Cheetham, R.K., Stephens, P.J., McBride, D.J., Humphray, S.J., Greenman, C.D., Varela, I., Lin, M.L., Ordóñez, G.R., Bignell, G.R., et al. (2010a). A comprehensive catalogue of somatic mutations from a human cancer genome. Nature *463*, 191–196.

Pleasance, E.D., Stephens, P.J., O'Meara, S., McBride, D.J., Meynert, A., Jones, D., Lin, M.L., Beare, D., Lau, K.W., Greenman, C., et al. (2010b). A small-cell lung cancer genome with complex signatures of tobacco exposure. Nature *463*, 184–190.

Poduri, A., Evrony, G.D., Cai, X., and Walsh, C.A. (2013). Somatic mutation, genomic variation, and neurological disease. Science *341*, 1237758.

Polak, P., and Arndt, P.F. (2008). Transcription induces strand-specific mutations at the 5′ end of human genes. Genome Res. *18*, 1216–1223.

Polak, P., Querfurth, R., and Arndt, P.F. (2010). The evolution of transcription-associated biases of mutations across vertebrates. BMC Evol. Biol. *10*, 187.

Polak, P., Lawrence, M.S., Haugen, E., Stoletzki, N., Stojanov, P., Thurman, R.E., Garraway, L.A., Mirkin, S., Getz, G., Stamatoyannopoulos, J.A., and Sunyaev, S.R. (2014). Reduced local mutation density in regulatory DNA of cancer genomes is linked to DNA repair. Nat. Biotechnol. *32*, 71–75.

Polak, P., Karlić, R., Koren, A., Thurman, R., Sandstrom, R., Lawrence, M.S., Reynolds, A., Rynes, E., Vlahoviček, K., Stamatoyannopoulos, J.A., and Sunyaev, S.R. (2015). Cell-of-origin chromatin organization shapes the mutational landscape of cancer. Nature *518*, 360–364.

Rhind, N., and Gilbert, D.M. (2013). DNA replication timing. Cold Spring Harb. Perspect. Biol. *5*, a010132.

Roberts, S.A., Lawrence, M.S., Klimczak, L.J., Grimm, S.A., Fargo, D., Stojanov, P., Kiezun, A., Kryukov, G.V., Carter, S.L., Saksena, G., et al. (2013). An APOBEC cytidine deaminase mutagenesis pattern is widespread in human cancers. Nat. Genet. *45*, 970–976.

Ross, K.A. (2014). Coherent somatic mutation in autoimmune disease. PLoS ONE *9*, e101093.

Ryba, T., Hiratani, I., Lu, J., Itoh, M., Kulik, M., Zhang, J., Schulz, T.C., Robins, A.J., Dalton, S., and Gilbert, D.M. (2010). Evolutionarily conserved replication timing profiles predict long-range chromatin interactions and distinguish closely related cell types. Genome Res. *20*, 761–770.

Shinbrot, E., Henninger, E.E., Weinhold, N., Covington, K.R., Göksenin, A.Y., Schultz, N., Chao, H., Doddapaneni, H., Muzny, D.M., Gibbs, R.A., et al. (2014). Exonuclease mutations in DNA polymerase epsilon reveal replication strand specific mutation patterns and human origins of replication. Genome Res. *24*, 1740–1750.

Spivak, G., and Ganesan, A.K. (2014). The complex choreography of transcription-coupled repair. DNA Repair (Amst.) *19*, 64–70.

Stillman, B. (2015). Reconsidering DNA Polymerases at the Replication Fork in Eukaryotes. Mol. Cell *59*, 139–141.

Supek, F., and Lehner, B. (2015). Differential DNA mismatch repair underlies mutation rate variation across the human genome. Nature *521*, 81–84.

Taylor, B.J., Nik-Zainal, S., Wu, Y.L., Stebbings, L.A., Raine, K., Campbell, P.J., Rada, C., Stratton, M.R., and Neuberger, M.S. (2013). DNA deaminases induce break-associated mutation showers with implication of APOBEC3B and 3A in breast cancer kataegis. eLife *2*, e00534.

Taylor, B.J., Wu, Y.L., and Rada, C. (2014). Active RNAP pre-initiation sites are highly mutated by cytidine deaminases in yeast, with AID targeting small RNA genes. eLife *3*, e03553.

Tomasetti, C., and Bozic, I. (2015). The (not so) immortal strand hypothesis. Stem Cell Res. (Amst.) *14*, 238–241.

Touchon, M., Nicolay, S., Audit, B., Brodie of Brodie, E.B., d'Aubenton-Carafa, Y., Arneodo, A., and Thermes, C. (2005). Replication-associated strand asymmetries in mammalian genomes: toward detection of replication origins. Proc. Natl. Acad. Sci. USA *102*, 9836–9841.

Trinklein, N.D., Aldred, S.F., Hartman, S.J., Schroeder, D.I., Otillar, R.P., and Myers, R.M. (2004). An abundance of bidirectional promoters in the human genome. Genome Res. *14*, 62–66.

Vilar, E., and Gruber, S.B. (2010). Microsatellite instability in colorectal cancer-the stable evidence. Nat. Rev. Clin. Oncol. *7*, 153–162.

Waddell, N., Pajic, M., Patch, A.M., Chang, D.K., Kassahn, K.S., Bailey, P., Johns, A.L., Miller, D., Nones, K., Quek, K., et al.; Australian Pancreatic Cancer Genome Initiative (2015). Whole genomes redefine the mutational landscape of pancreatic cancer. Nature *518*, 495–501.

Wang, L., Lawrence, M.S., Wan, Y., Stojanov, P., Sougnez, C., Stevenson, K., Werner, L., Sivachenko, A., DeLuca, D.S., Zhang, L., et al. (2011). SF3B1 and other novel cancer genes in chronic lymphocytic leukemia. N. Engl. J. Med. *365*, 2497–2506.

Yadlapalli, S., and Yamashita, Y.M. (2013). DNA asymmetry in stem cells - immortal or mortal? J. Cell Sci. *126*, 4069–4076.

Yu, C., Gan, H., Han, J., Zhou, Z.X., Jia, S., Chabes, A., Farrugia, G., Ordog, T., and Zhang, Z. (2014). Strand-specific analysis shows protein binding at replication forks and PCNA unloading from lagging strands when forks stall. Mol. Cell *56*, 551–563.